Turkish Journal of Chemistry
http://journals.tubitak.gov.tr/chem/
Research Article

Turk J Chem
(2014) 38: 260 – 274

doi:10.3906/kim-1212-76

Effect of boric acid on corrosion and electrochemical performance of Pb-0.08% Ca-1.1% Sn alloys containing Cu, As, and Sb impurities for manufacture of grids of lead-acid batteries

Said SALIH, Ahmed GAD-ALLAH, Ashraf ABD EL-WAHAB, Hamid ABD EL-RAHMAN*
Chemistry Department, Faculty of Science, Cairo University, Giza, Egypt

Received: 31.12.2012 • **Accepted:** 11.09.2013 • **Published Online:** 14.03.2014 • **Printed:** 11.04.2014

Abstract: The electrochemical performance of lead-acid batteries made of Pb–Ca–Sn alloys with and without 0.1% of each of Cu, As, and Sb individually and combined in 4.0 M H_2SO_4 in the absence and presence of 0.4 M H_3BO_3 was studied. Both impurities and H_3BO_3 were found to reduce the corrosion rate. Cyclic voltammetry revealed that the presence of impurities or H_3BO_3 significantly retarded the formation of large crystal $PbSO_4$. H_3BO_3 increased the rates of oxygen and hydrogen evolution reactions for all alloys. Impedance measurement was used to quantify the amounts of $PbSO_4$ and PbO in the initial stage of the oxidation. H_3BO_3 decreased the positive grid corrosion of all alloys, while impurities increased it. Although impurities increased the self-discharge during constant current discharge, H_3BO_3 was found to decrease it, except for the alloy containing the 3 impurities and the Cu-containing alloy. Under open-circuit conditions, H_3BO_3 increased significantly the self-discharge rate, but impurities were found to suppress it.

Key words: Pb–Ca–Sn alloys, lead-acid batteries, recycled lead, boric acid

1. Introduction

Various electrolyte additives have been investigated in order to improve the electrochemical performance of lead-acid batteries, including metal ions.[1–10] Phosphoric acid is the most frequently studied electrolytic additive, with positive and negative effects on battery performance.[11–35] H_3PO_4 was found to reduce sulfation, especially after deep discharge,[12,13,17,22] increase the battery cycle life,[28] and slow down self-discharge.[20,23] The serious disadvantage of addition of H_3PO_4 was found to be a loss in cell capacity.[21] The effect of H_3PO_4 on the efficiency of formation of PbO_2 on the positive grid during charging was found to depend on the charging conditions; some conditions increased the efficiency,[16,25] while others showed the opposite effect.[21,23,34] Citric acid as an electrolytic additive was reported to decease the self-discharge of lead-acid batteries by the suppression of PbO_2 reduction.[36,37] Little attention has been given to boric acid as an electrolytic additive.[29,37–39] A mixture of H_3BO_3 + H_3PO_4, among other binary additives, suppressed the corrosion of lead electrodes of a lead-acid battery and the results were explained in terms of H^+ ion transport and the morphology change of the $PbSO_4$ layer.[29] H_3BO_3 has been assumed to decrease the self-discharge of PbO_2 by inhibiting its transformation into $PbSO_4$.[38] Washing of positive grids made of Pb-1.7% Sb in 1 wt% H_3BO_3 eliminated the rapid decline in the initial discharge voltage due to the resistive $PbSO_4$ layer.[39]

*Correspondence: abdelrahman_hamid@hotmail.com

Most pig lead used in the manufacture of grids is provided by the recycling of lead batteries and other lead products.[40–42] According to ASTM Designation B29-79(84) and the Battery Council International (BCI), a tolerance level less than 20 mg/kg is recommended for elemental impurities, such as As, Cu, and Sb, in pig lead for the manufacture of grids. The elements As, Cu, and Sb are usually added as minor alloying elements in many lead-based alloys to impart specific properties, and hence they are potential impurities in most recycled lead products. The use of recycled lead with impurity levels above those in the industrial standards would be interesting from the environmental and economic points of view. Grids based on Pb–Ca alloys dominate the market of valve-regulated lead-acid batteries due to their superior properties. It is hoped that the possible harmful effect of As, Cu, and Sb impurities may be compensated for by the addition of H_3BO_3.

In the present work, the effect of 0.4 M H_3BO_3 on the electrochemical performance of the commercial Pb-0.08% Ca-1.1% Sn alloys containing 0.1 wt% of Cu or As or Sb or the 3 elements combined was studied in 4.0 M H_2SO_4.

2. Experimental

Disc working electrodes were cut from rods of commercial Pb–Ca–Sn alloys with and without various elemental additions. The composition wt% of the commercial Pb–Ca–Sn alloy (alloy G-0) was as follows: Sn 1.1214, Sb 0.00033, Cu 0.00034, As 0.00019, Ca 0.08279, and Pb 98.7807. Four impurity-containing alloys were made by addition of the respective element(s) during casting: 0.1 wt% As (alloy G-As), 0.1 wt% Cu (alloy G-Cu), 0.1 wt% Sb (alloy G-Sb), and 0.1 wt% As + 0.1 wt% Cu + 0.1 wt% Sb (alloy G-ACS). A 2-cm-long rod of the alloy was coated with a thin epoxy adhesive (Araldite®, Ciba, Switzerland) and inserted in thick-walled glass tubing with appropriate cross-sectional area. The cross-sectional area of the alloy, ca. 0.28 cm^2, was only left in contact with the test solution. A stout copper rod was screwed to the other end of the alloy rod to provide the electrical contact of the electrode. The electrodes were mechanically polished with successive grades of emery papers up to 1200 grit, then washed with acetone and double distilled water, and finally cleaned with a fine tissue so that the surface appeared bright and free from defects. A 3-electrode cell was employed in all electrochemical tests. The counter electrode was a platinum sheet of area ca. 2×2 cm^2 positioned in the cell to face the working disc electrode. The potential of the alloy electrode was measured versus an $Hg/Hg_2SO_4/1.0$ M H_2SO_4 reference electrode (0.680 V vs. SHE). All potentials are given relative to the previously mentioned reference electrode. Chemically ultrapure sulfuric acid 98% stock and ultrapure H_3BO_3 were used for preparation of solutions by appropriate dilution using doubly distilled water. All measurements were conducted in unstirred naturally aerated 4.0 M H_2SO_4 acid solutions with and without 0.4 M H_3BO_3 at a constant temperature of 25 ± 0.2 °C.

The different electrochemical measurements were carried out using the electrochemical system IM6 Zahner electric, Meßtechink, Germany. Impedance was measured at a frequency, f, of 1.0 kHz using an AC potential of 3 mV peak to peak. With the large counter electrode used, the cell impedance was reduced to that of the working electrode and the solution resistance between the working and counter electrodes. The electrode capacitance, C (F), and resistance, R (Ω), values were extracted from the impedance, Z (Ω), and the phase shift angle, θ values of the cell: $Z = \sqrt{R^2 + (1/2f\pi C)^2}$ and $\tan\theta = 1/2\pi fRC$. Cyclic voltammetry was carried out by scanning potential from –1.9 V to 2.0 V at a scan rate of 10 mV s^{-1}. Constant current oxidation/reduction (or in the terminology of rechargeable batteries charging/discharging) curves were formed by applying a cathodic current of 0.54 mA cm^{-2} for 5 min to remove any reducible species from the alloy surface and then the current

polarity was reversed to oxidize the alloy for 60 min. Finally, the current polarity was again reversed to reduce the formed PbO_2 on the alloy surface. The reduction continued until the H_2 evolution potential was attained. In the self-discharge tests, the alloys were anodized for 30 min at 0.54 mA cm^{-2} and then the circuit was opened and the open-circuit potential and impedance were recorded until the PbO_2 on the alloys was fully self-discharged to $PbSO_4$.

3. Results and discussion

3.1. Effect of H_3BO_3 on corrodibility of grids

Figure 1 shows Tafel plots for Pb-0.08% Ca-1.1% Sn alloys with and without impurities in 4.0 M H_2SO_4 with and without 0.4 M H_3BO_3. The shape of the Tafel plots is the same for all alloys in the 2 solutions. The presence of H_3BO_3 causes a vertical shift in the position of Tafel plots towards less negative potentials. The corrosion current, i_{corr}, corrosion potential, E_{corr}, and the cathodic and anodic Tafel slopes, b_c and b_a, are given in Table 1. The anodic branches show a clear active–passivation transition due to the growth of a barrier $PbSO_4$ layer.[43,44] The passivation current, i_p, in Table 1 is taken at overpotential of 175 mV to make a comprehensive comparison between the absence and presence of H_3BO_3.

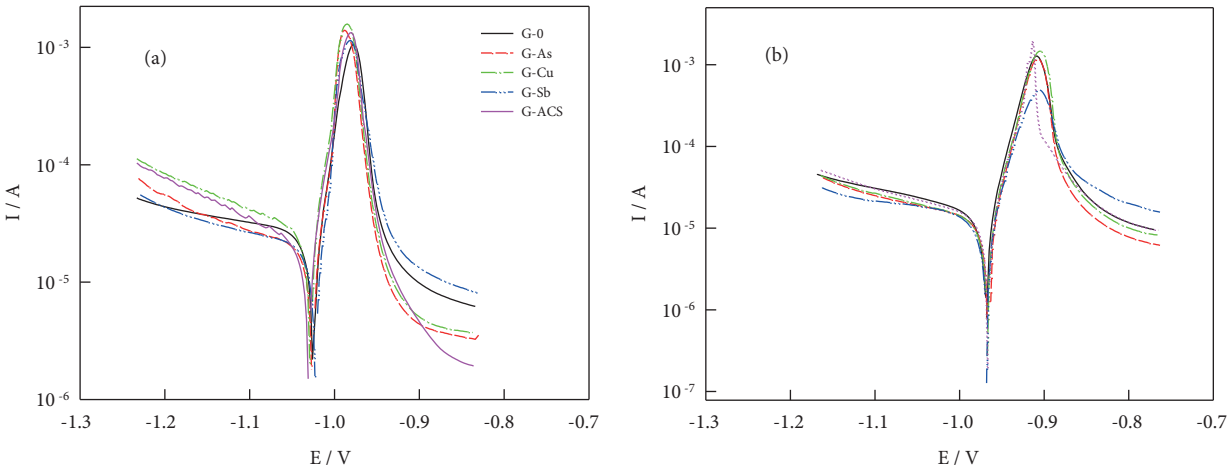

Figure 1. Tafel plots for Pb–Ca–Sn alloys with and without different impurities in 4 M H_2SO_4 in the absence (a) and the presence of 0.4 M H_3BO_3 acid (b).

In the absence of H_3BO_3, E_{corr} for alloy G-0 is close to the equilibrium potential, E_{eq}, of the following redox electrode in 4.0 M H_2SO_4:[43,44]

$$PbSO_4 + 2e \rightleftharpoons Pb + SO_4^{2-}; \quad E_{eq} = -1.04V \tag{1}$$

E_{corr} shifts slightly to less negative values in the presence of impurities (7–17 mV), indicating enhancement of the passivation properties of the naturally formed $PbSO_4$ layer on the corroding alloys. In the presence of H_3BO_3, E_{corr} becomes less negative by $\sim$ 60 mV, depending on alloy composition. E_{corr} shift in the positive direction may be attributed to passivity enhancement in boric acid-containing H_2SO_4 solutions and/or a rise in solution acidity. The rise in acidity is expected to shift the equilibrium potential of hydrogen or oxygen electrode (cathodic half-cell in corrosion process), and consequently E_{corr} shifts in the positive direction. The fact that i_p in the presence of H_3BO_3 is clearly higher than in its absence indicates that H_3BO_3 is not a

passivity enhancer. It is interesting that the Sb-containing alloy G-Sb has the highest i_p values, while the As-containing alloy G-As has the lowest i_p, in the absence and presence of H_3BO_3. It is assumed that Sb_2O_3 in the passive film of alloy G-Sb dissolves more rapidly, making the passive film more porous and less protective than in other alloys. In contrast, As_2O_3 in the passive film of alloy G-As resists dissolution and reinforces the passive film, making the passive film less porous and more protective more than in other alloys.

Table 1. Corrosion data from Tafel plots for Pb–Ca–Sn alloys with and without different impurities in 4 M H_2SO_4 in the absence and presence of 0.4 M H_3BO_3.

Parameter	G-0	G-As	G-Cu	G-Sb	G-ACS
Absence of H_3BO_3					
E_{corr}/V	–1.026	–1.019	–1.012	–1.014	–1.019
i_{corr}/μA cm^{-2}	126.8	61.1	84.3	65.7	50.7
b_c/V	0.926	0.389	0.786	0.538	0.247
b_a/V	0.027	0.018	0.013	0.014	0.017
i_{pass}/μA cm^{-2}	23.9	12.1	13.6	32.1	7.5
Presence of H_3BO_3					
E_{corr}/V	–0.959	–0.956	–0.960	–0.957	–0.959
i_{corr}/μA cm^{-2}	52.5	30.4	41.4	50.0	45.4
b_c/V	0.433	0.343	0.389	0.750	0.368
b_a/V	0.019	0.023	0.021	0.026	0.021
i_{pass}/μA cm^{-2}	38.6	25.4	33.2	67.5	38.9

The presence of H_3BO_3 or impurities affects the slope of the cathodic branch more significantly than the anodic one. Thus, corrosion of Pb-0.08% Ca-1.1% Sn alloys in the absence and presence of H_3BO_3 is assumed to occur under predominantly cathodic control. The presence of impurities in the alloy leads to a decrease in i_{corr} (33%–60%). Moreover, the presence of H_3BO_3 in solution leads to a decrease in i_{corr} (59%–76%).

3.2. Effect of H_3BO_3 on cyclic voltammetry of grids

Figure 2 shows cyclic voltammograms (CVs) for Pb-0.08% Ca-1.1% Sn alloys with and without impurities in 4.0 M H_2SO_4 in the absence and presence of 0.4 M H_3BO_3. In one and the same solution, all alloys showed the same features with differences in the magnitudes of the redox peaks. No redox peaks related to the impurity element(s) were detected. CVs reflect only the redox peaks related to Pb component in the alloys and they are similar to those previously reported.[45–53]

The significant effects of H_3BO_3 on CVs are:

- Appearance of a new small anodic peak, A2. Peak A2 is most pronounced for alloy G-Sb. The potential of peak A2 is close to the equilibrium potential of the following redox processes:[34,43]

$$3PbOPbSO_4 + 6H^+ + 8e \rightleftharpoons 4Pb + SO_4^{2-} + 4H_2O; \quad E_{eq} = -0.66V \tag{2}$$

$$PbOPbSO_4 + 2H^+ + 4e \rightleftharpoons 2Pb + SO_4^{2-} + H_2O; \quad E_{eq} = -0.8V \tag{3}$$

  Thus, peak A2 is attributed to the formation of basic lead sulfates according to Eqs. (2) and (3).

- All redox peaks slightly shift in the anodic direction, most probably due to acidity change as mentioned in part 3.1.

- Significant suppression of peak C_4 (overlaps with the hydrogen evolution for alloy G-0)

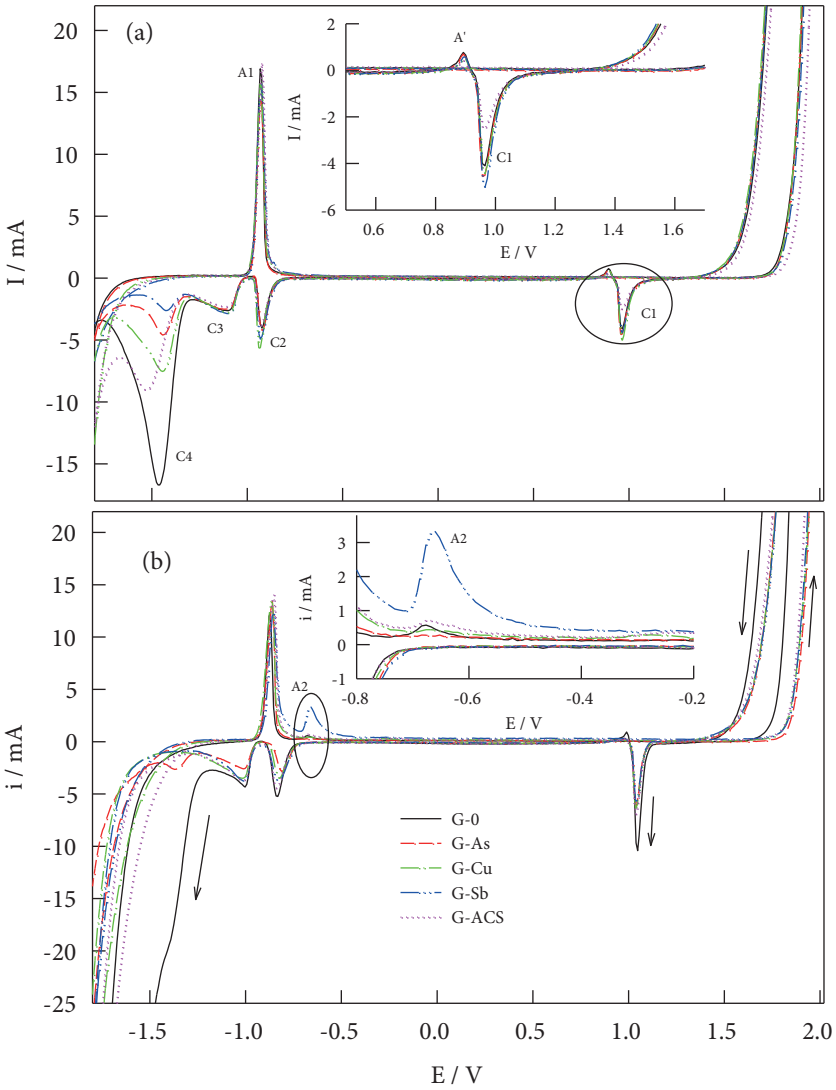

Figure 2. Cyclic voltammograms of Pb–Ca–Sn alloys with and without different impurities in 4 M H_2SO_4 in the absence (a) and the presence of 0.4 M H_3BO_3 acid (b). Insets are magnifications of the circled parts of the main curves.

The redox peak A1 is attributed to the formation and growth of a $PbSO_4$ layer on the alloy surface. The passivity region extends from –0.5 V to 1.7 V until the onset of oxygen evolution with concurrent PbO_2 formation. On reversing the potential scan, the formed PbO_2 is reduced in several steps to Pb (C1–C4). Peak C1 is attributed to the electro-reduction of PbO_2 to $PbSO_4$. When PbO_2 is reduced to $PbSO_4$, a large increase in molar volume is expected and, as a result, the surface cracks, exposing the bare metal. The parts of the bare surface are then oxidized in the anodic excursion peak A'.[50,54]

Peak C2 is attributed to the reduction of PbO to Pb and peaks C3 and C4 are connected to reduction of small and large crystals of $PbSO_4$ to Pb, respectively.[48] The peak potentials of C2–C4 occur at significantly more negative potentials than the reversible potentials for the couples $PbOPbSO_4$/Pb and $PbSO_4$/Pb, respec-

tively. This is probably due to the insulating nature of these compounds, which leads to a large ohmic drop and hence peak potential shifts to more negative potentials.

It is obvious that the amount of charge consumed in Pb^{4+} to Pb^{2+} reduction (peak C1) is much lower than the charge consumed in Pb^{2+} to Pb (peaks C2–C4). This is mainly attributed to the strong contribution of the self-discharge of PbO_2 with the underlying Pb in the alloys.[34,35] Moreover, the anodic process at A' adds more Pb^{2+} species. The self-discharge occurs spontaneously according to the following comproportionation reaction:[34,35,43,44]

$$PbO_2 + Pb + 2H_2SO_4 \rightarrow 2PbSO_4 + 2H_2O \quad (4)$$

H_3BO_3 significantly suppresses peak C4 for all alloys, except for alloy G-0. This indicates that both impurities and H_3BO_3 suppress the formation of large crystals of $PbSO_4$.

3.3. Effect of H_3BO_3 on hydrogen and oxygen evolution reactions

In the constant current charging process of a battery and as the potential of the full charge capacity is reached, water decomposition to H_2 gas at the negative grid and O_2 gas at the positive grid becomes the predominating process. Without proper recombination of H_2 and O_2 to water, as in good valve-regulated lead-acid batteries (VRLAB), water loss problems occur. Alloys with high overpotentials for H_2 and O_2, at a specific current, are desirable to avoid water and energy losses. Alternatively, alloys with lower currents, at constant and sufficiently high overpotential, are preferred.

Figure 3 shows polarization curves for the hydrogen evolution reaction (HER) and the oxygen evolution reaction (OER) on Pb-0.08% Ca-1.1% Sn alloys in 4.0 M H_2SO_4 in the absence and presence of 0.4 M H_3BO_3. The Tafel slope for HER depends significantly on the alloy composition in the absence of H_3BO_3 (0.136–0.230 V decade^{-1}) but it becomes higher and practically independent on the alloy type in the presence of H_3BO_3 (0.259–0.330 V decade^{-1}). It is known that the HER on pure Pb occurs according to a proton discharge-rate determining step followed by a fast electrodic desorption step, with a typical Tafel slope of 118 mV decade^{-1} at 25 °C. Grains containing the minor alloying elements, especially Sb, in the surface of the alloys may act as new centers for the HER and significantly change the mechanism of the HER, leading to the observed higher Tafel slopes. Furthermore, the contribution of diffusion, especially in the presence of H_3BO_3, may account for the imperfect Tafel lines and their higher slopes.

The kinetics of the oxygen evolution reaction (OER) is more difficult to deduce because of the concurrent PbO_2 formation during an OER at high anodic potentials. A simple procedure was used in the present work to suppress oxide formation, by holding the potential at 2.0 V for 10 min before scanning the potential in the cathodic direction until 1.2 V. As can be seen in Figure 3, linear Tafel plots over more than 2 decades of current for OER could be obtained, although the linearity region in the presence of H_3BO_3 is shorter. The fact that Tafel plots are almost parallel indicates that the OER mechanism is independent on the alloy type. The Tafel slope for OER in the absence of H_3BO_3 (0.170–0.179 V decade^{-1}) is lower than in the presence of H_3BO_3 (0.191–0.215 V decade^{-1}), except for alloy G-0 (0.131 V decade^{-1}). Figure 4 shows the dependence of the currents of HER (at –1.9 V) and OER (at 1.9 V) on the alloy type in the absence and presence of H_3BO_3. H_3BO_3 significantly increases the rates of OER and HER for all alloys. The percentages of increase in the rates of both HER and OER, I_{H_2}% and I_{O_2}%, due to the presence of H_3BO_3 indicate that the minimum harmful effect of H_3BO_3 is for alloy G-Cu. The maximum harmful effect of H_3BO_3 is for alloy G-0, since it speeds up both the OER and HER.

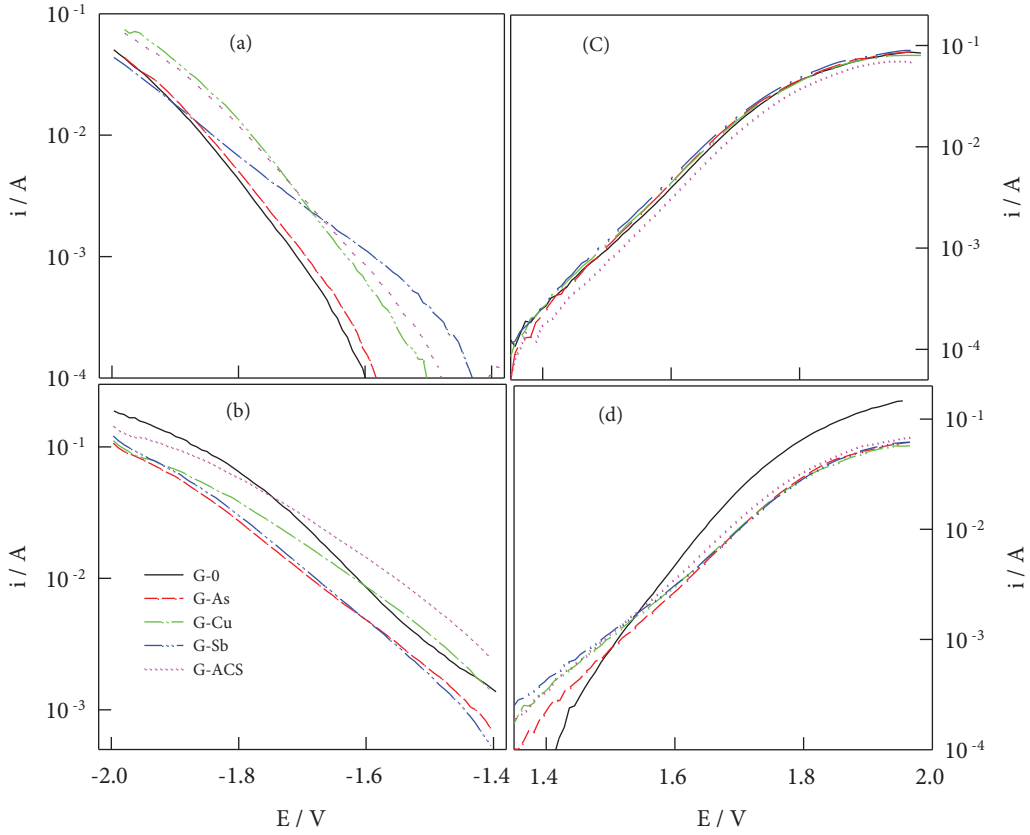

Figure 3. Cathodic polarization curves of hydrogen evolution reaction (a and b) and anodic polarization curves for oxygen evolution (c and d) on Pb–Ca–Sn alloys in 4 M H_2SO_4 in the absence (a and c) and the presence of 0.4 M H_3BO_3 acid (b and d).

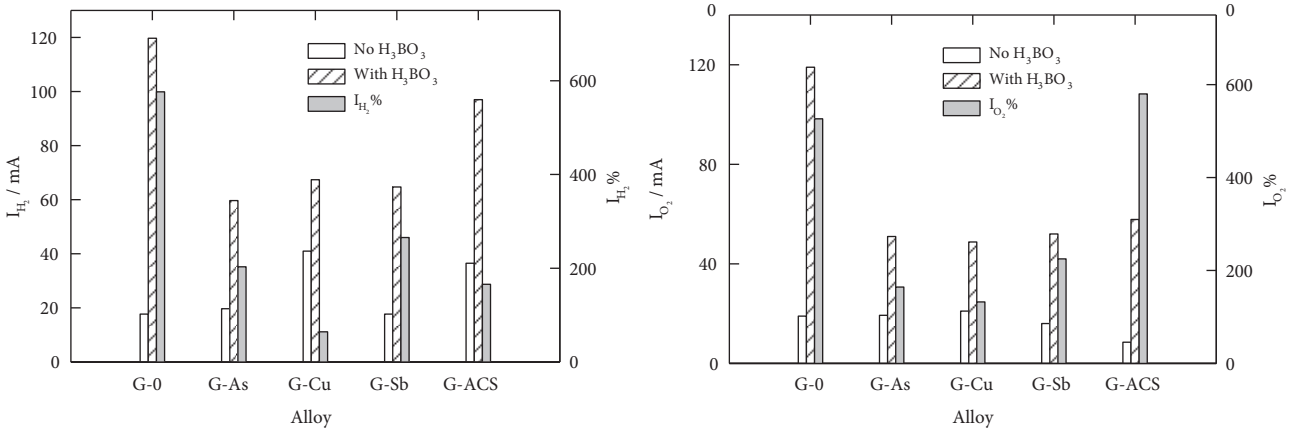

Figure 4. Dependence of the currents of HER at –1.9 V and OER at 1.9 V on alloy type.

3.4. Effect of H_3BO_3 on constant current charging/discharging

Figure 5 shows the instantaneous variations in potential, capacitance, and resistance during the galvanostatic anodic (charging)/cathodic (discharging) polarization of Pb-0.08% Ca-1.1% Sn alloy at 0.54 mA cm^{-2} in

4.0 M H_2SO_4 in the presence of 0.4 M H_3BO_3. The curves for alloy G-0 in the absence of H_3BO_3 are added for comparison. The rest of the alloys showed the same features. Due to its large change during charging/discharging, C is shown on a logarithmic scale for better resolution. The main features of polarization curves in the absence and presence of H_3BO_3 are the same.

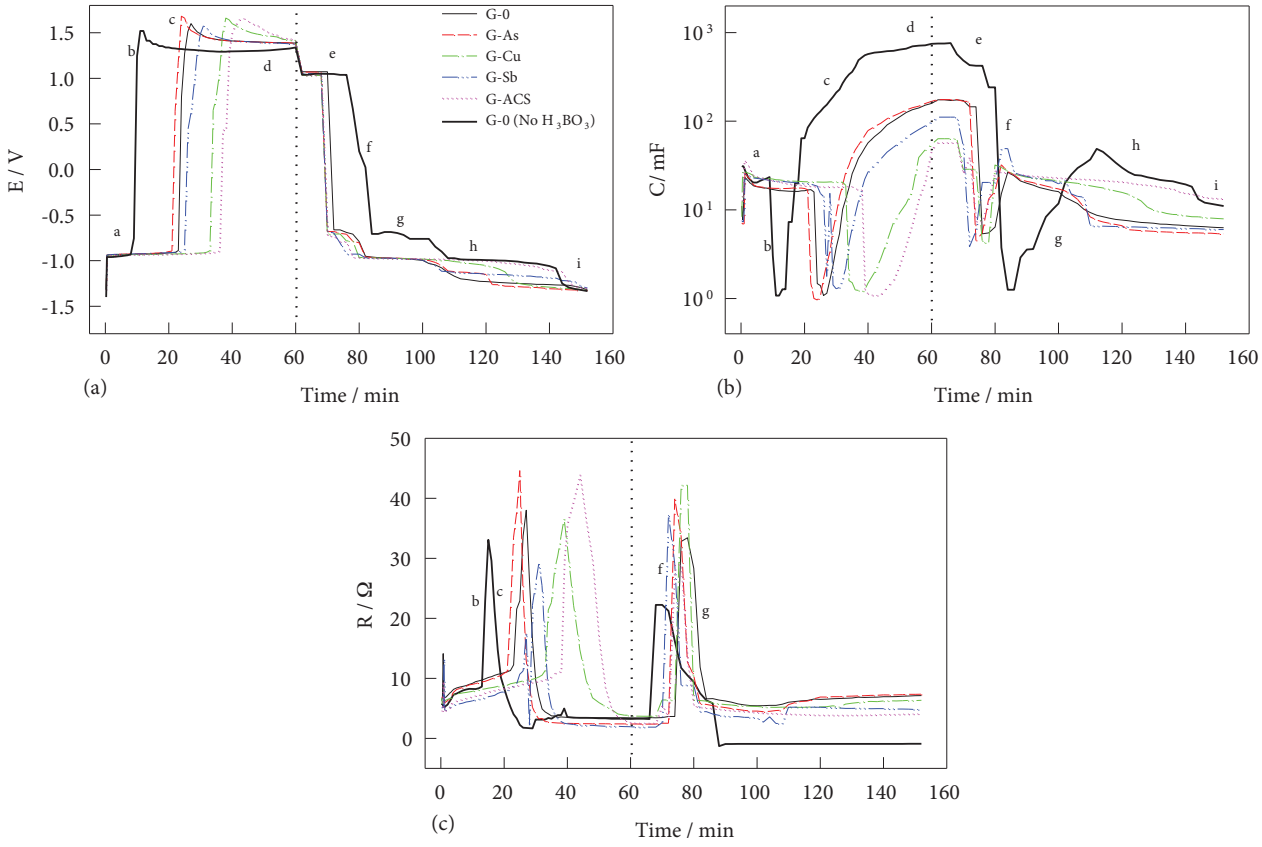

Figure 5. Instantaneous potential, E, capacitance, C, and resistance, R, during the galvanostatic oxidation/reduction of Pb–Ca–Sn alloys at 0.54 mA in 4 M H_2SO_4 in the presence of 0.4 M H_3BO_3 acid. Bold lines refer to alloy G_0 in the absence of H_3BO_3. The vertical dotted line refers to the start of reduction.

The oxidation process involves 4 stages (a–d). Stage a: $PbSO_4$ formation during arrest at –0.96 V and –0.93 V in the absence and presence of H_3BO_3, respectively. It is slightly more positive than the equilibrium potential of the redox $Pb/PbSO_4$.[34,43,44]

In this stage, C decreases slightly and slowly. Concurrently R increases with time. The results are consistent with the growth of an insulating $PbSO_4$ film on the alloy surface. The duration of this stage depends on the impurity type and is used for calculation of the amount of charge consumed during the formation of $PbSO_4$, $Q^f_{PbSO_4}$. Stage b: A sharp increase in E to ~1.5 V, depending on impurity type. A corresponding sharp decrease in C to a minimum (~1 μF) and a sharp increase in R to a maximum occur. This behavior is attributed to the formation of a highly insulating inner PbO film beneath the $PbSO_4$ layer.[34,49]

The formation of an inner PbO layer occurs as a result of acidity depression via retardation of the diffusion of H_2SO_4 through the outer $PbSO_4$ film. The time needed to reach the minimum C or maximum R is the same and it is used in calculation of the amount of charge consumed in the formation of PbO, Q^f_{PbO}. Stage c:

E decreases slowly to more or less stationary values. C increases very sharply and R decreases to the solution resistance, indicating the transformation of PbO and $PbSO_4$ to the conducting PbO_2. Stage d, E stays more or less invariant while C increases but with a slower rate than in region c due to the strong contribution of OER, beside the growth of PbO_2.

The reduction (discharge) process involves several stages (e–i). Stage e: The electro-reduction of PbO_2 to $PbSO_4$ at 1.0 V.[34,43] C increases in the initial stage of reduction to a maximum and then it decreases, while R stays low. The initial increase in C is attributed to an increase in the dielectric properties of the PbO_2 layer as a result of the concurrent OER and involvement of O_2 species in the growing PbO_2 layer.[34] The later decrease in C is connected to a decrease in the dielectric properties of the surface layer as a result of electro-transformation of the conducting PbO_2 into the insulating $PbSO_4$.

Stage f: A sharp decrease in E and C and an increase of R are noted. This stage ends with a minimum C and a maximum R. This reduction stage signifies the formation of an inner insulating PbO layer beneath $PbSO_4$ at the alloy/film interface. The time of stage e is used in calculation of the amount of charge consumed during the reduction of PbO_2, $Q^r_{PbO_2}$. Stage g: The reduction of basic lead sulfates, $PbO \cdot PbSO_4$ and $3PbO \cdot PbSO_4$, to Pb at $\sim$ –0.7 V (sometimes ill-definite) occurs according to processes (2) and (3). A considerable increase in C and a decrease in R are noted in this stage and attributed to the transformation of the insulting PbO and $PbSO_4$ into the conducting Pb. Stage h: $PbSO_4$ is reduced to Pb at $\sim$ –1.0 V with a slow decrease in C. The times of stages g and h are used for calculation of the amounts of charges consumed during the reduction of basic lead sulfates, Q^r_{BLS} and $PbSO_4$, $Q^r_{PbSO_4}$, respectively. Stage i: E shifts to a more negative potential ($\sim$ –1.2 V) where H_2 evolves. In this stage, there is a decrease in C and a slight increase in R, probably due to the H_2 bubbles evolved.

The charges consumed in various oxidation reduction processes in the absence and presence of H_3BO_3 are summarized in Table 2. The large difference between $Q^r_{PbO_2}$ and $Q^r_{BLS} + Q^r_{PbSO_4}$ is attributed to the self-discharge of PbO_2 according to process (3). The charge loss due to self-discharge during the reduction, Q^r_{SD}, was estimated according to the relation:

$$Q^r_{SD} = 0.5(Q^r_{BLS} + Q^r_{PbSO_4}) - Q^r_{PbO_2} \tag{5}$$

The charge consumed in the formation of PbO_2, Q^f_{PbO2}, was calculated according to the relation:

$$Q^f_{PbO_2} = 2\left(Q^r_{PbO_2} + Q_{SD}\right) \tag{6}$$

PbO_2 is considered the final corrosion product in the oxidation process of alloys, and the rate of positive grid corrosion, PG_{corr} (g cm^{-2} h^{-1}), was calculated from $Q^f_{PbO_2}$ as follows:

$$PG_{corr} = Q^f_{PbO_2} \times 207.19/4Ft, \tag{7}$$

where the value 207.19 is the atomic mass of Pb and time t = 1 h. The dependence of $Q^f_{PbSO_4}$, Q^f_{PbO2}, Q^r_{SD}, and PG_{corr} on alloy type in the absence and presence of H_3BO_3 is shown in Figure 6. The presence of H_3BO_3 leads to:

Table 2. Charge densities consumed in the various redox processes in the charging/discharging of Pb–Ca–Sn alloys at 0.54 mA cm^{-2} in 4.0 M H_2SO_4 in the absence and presence of 0.4 M H_3BO_3.

Charge/C cm^{-2}	G-0	G-As	G-Cu	G-Sb	G-ACS
Absence of H_3BO_3					
$Q^f_{PbSO_4}$	0.194	0.151	0.324	0.259	0.259
Q^f_{PbO}	0.086	0.065	0.043	0.065	0.043
$Q^r_{PbO_2}$	0.497	0.346	0.346	0.259	0.410
Q^r_{BLS}	0.518	0.605	0.303	0.626	0.432
$Q^r_{PbSO_4}$	0.734	0.972	1.188	0.994	1.080
$Q^f_{PbO_2}$	1.751	1.920	1.842	1.881	1.922
Q^r_{SD}	0.378	0.616	0.573	0.681	0.551
Presence of H_3BO_3					
$Q^f_{PbSO_4}$	0.680	0.616	1.004	0.745	1.101
Q^f_{PbO}	0.194	0.194	0.259	0.259	0.324
$Q^r_{PbO_2}$	0.259	0.194	0.194	0.194	0.194
Q^r_{BLS}	0.130	0.194	0.162	0.097	0.162
$Q^r_{PbSO_4}$	0.583	0.777	1.231	0.907	1.361
$Q^f_{PbO_2}$	0.972	1.166	1.588	1.198	1.718
Q^r_{SD}	0.227	0.389	0.600	0.405	0.665

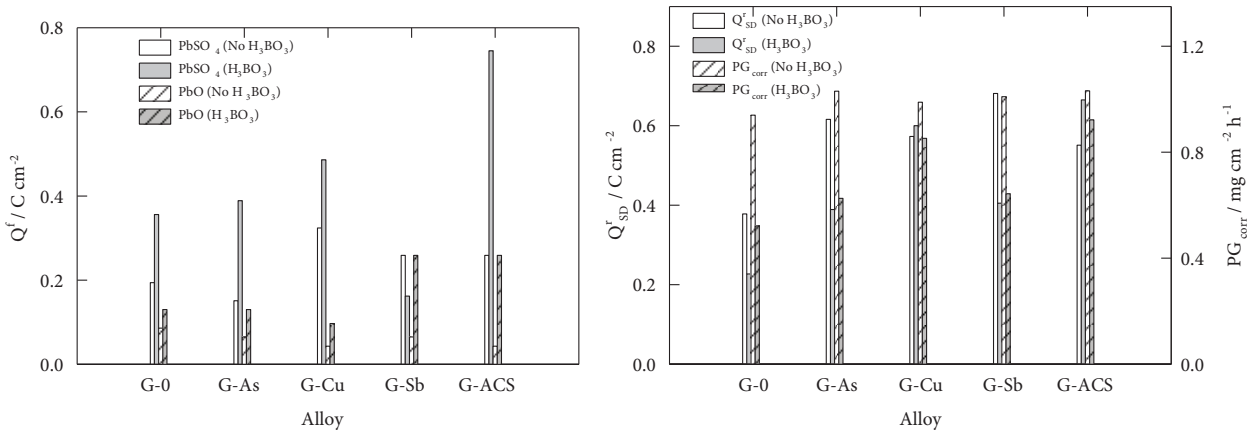

Figure 6. Dependence of the charge of formation, Q^f, and both the self-discharge charge, Q^r_{SD}, and the positive grid corrosion, PG_{corr}, on alloy type.

- An increase in amount of PbO formed during charging for all alloys (51%–502%), especially for alloys G-Sb (298%) and G-ACS (502%).

- An increase in amount of $PbSO_4$ formed during charging for all alloys (84%–188%), except for alloy G-Sb (37% decrease).

- A decrease in the positive grid corrosion for all alloys (11%–44%). The positive grid corrosion rate is the lowest for alloy G-0 in the absence and presence of H_3BO_3.

- An apparent decrease in self-discharge during reduction for all alloys (21%–41%), except for alloys G-ACS (21% increase) and G-Cu (5% increase). The effect of H_3BO_3 on self-discharge can be explained in terms

of the amount of PbO_2 formed and/or the morphological changes in PbO_2.[29,38] To clarify this point, the dependence of self-discharge on the amount of PbO_2 is represented in Figure 7, using Q^r_{SD} and Q^f_{PbO2} given in the table for all alloys. As can be seen, there is actually a strong dependence of self-discharge on the amount of PbO_2 in the absence and presence of H_3BO_3. At a constant amount of PbO_2 (in terms of Q^f_{PbO2}), however, self-discharge in the presence of H_3BO_3 is significantly higher. Thus, the facilitation of self-discharge of PbO_2 in the presence of H_3BO_3 is attributed to the effect of H_3BO_3 on the morphology of PbO_2, when the amount of PbO_2 is kept constant.

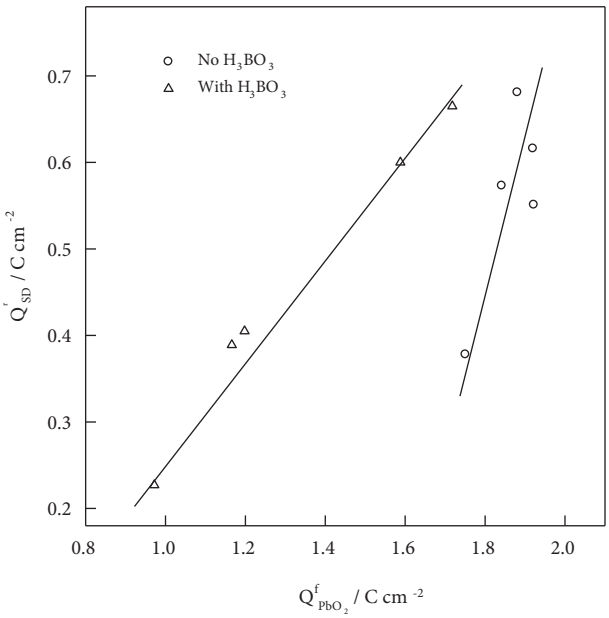

Figure 7. Variation in the self-discharge charge, Q^r_{SD}, with the charge of PbO_2 formation, $Q^f_{PbO_2}$.

3.5. Effect of H_3BO_3 on self-discharge of PbO_2 on grids

Figure 8 shows the variation in the open-circuit potential, E_{oc}, capacitance, C_{oc}, and resistance, R_{oc}, of the pre-oxidized alloys with time in 4.0 M H_2SO_4 in the absence and presence of 0.4 M H_3BO_3. The self-discharge curves for alloy G-0 in the absence of H_3BO_3 are also shown for comparison. The rest of the alloys in the absence of H_3BO_3 revealed the same features of curves shown in Figure 8. Time is shown on a logarithmic scale to allow better representation of the initial stage of the open-circuit self-discharge of PbO_2. Three hours are needed for full self-discharge of the PbO_2 layer on the alloy surface to $PbSO_4$, where E_{oc} varies from an initial potential of 1.2 V to a final potential of –1.0 V. At the beginning, E_{oc}, C_{oc}, and R_{oc} stay almost invariant with time for a period that depends on the alloy type. This period is significantly longer in the absence of H_3BO_3 and C_{oc} is much higher. One can infer that the amount of PbO_2 formed after 30 min of oxidation is considerably lower in the presence of H_3BO_3. At potential $\geq$1.0 V a slight change in C_{oc} is noted, and the transformation of PbO_2 to $PbSO_4$ is assumed.[34,43,44] Then E_{oc} rapidly decays to less positive values. A substantial decrease in C and an increase in R are seen during the rapid E_{oc} decay. These variations are attributed to the self-discharge of the inner PbO_2 layer to PbO via the reaction of the inner PbO_2 layer with the underlying Pb on the alloy surface according to the process:

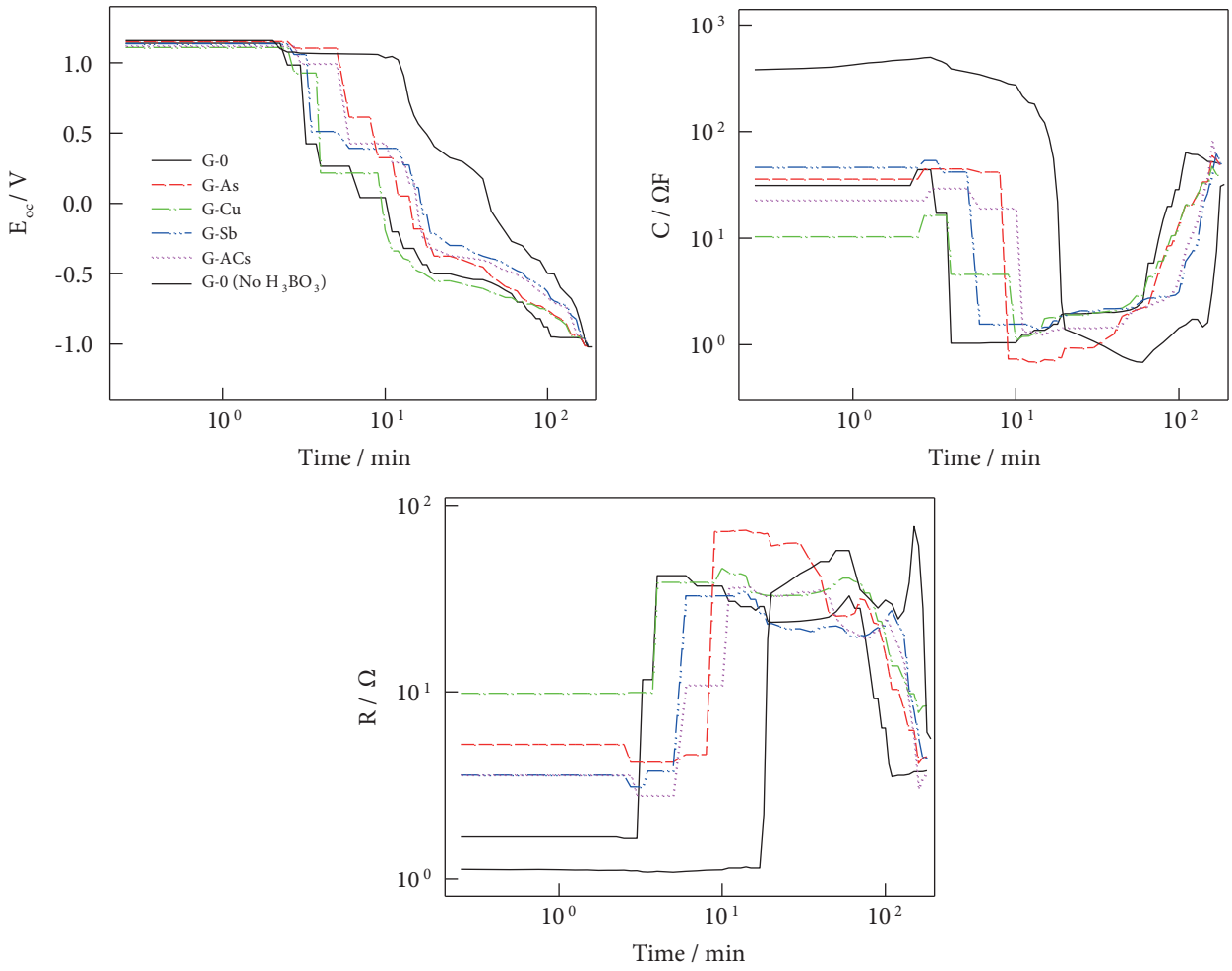

Figure 8. Instantaneous open-circuit potential, E_{oc}, capacitance, C_{oc}, and resistance, R_{oc}, during the self-discharge of alloys in 4.0 M H_2SO_4 + 0.4 H_3BO_3. The alloys were pre-oxidized at 0.54 mA for 30 min. Bold lines refer to alloy G_0 in the absence of H_3BO_3.

$$PbO_2 + Pb \rightleftharpoons 2PbO \tag{8}$$

At $E_{oc} \sim -0.3$ V, C increases and R decreases irregularly. The latter variations in C and R are attributed to the chemical transformation of the inner PbO layer into $PbSO_4$ as a result of diffusion of H_2SO_4 into the passive film:[49]

$$PbO + H_2SO_4 \rightleftharpoons PbSO_4 + H_2O. \tag{9}$$

The reciprocal of the time required to start the rapid decay at $E_{oc} = 1.0$ V, t_{SD}^{-1}, was taken as a measure for the self-discharge rate under open-circuit conditions. Figure 9 shows that H_3BO_3 significantly increases t_{SD}^{-1} for all alloys. The percentage of the relative increase in self-discharge due to the presence of H_3BO_3, RSD%, follows the order: G-0 >> G-Cu > G-ACS > G-As > G-Sb. Thus, the presence of impurities, especially Sb and As, seems to retard the harmful effect of H_3BO_3.

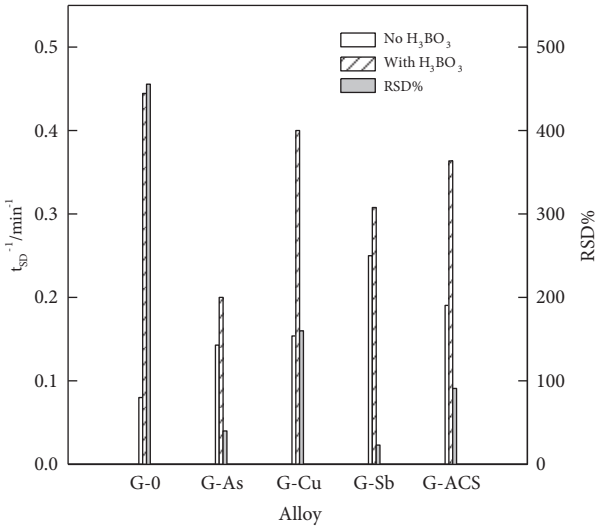

Figure 9. Dependence of the self-discharge rate, t_{SD}^{-1}, and the percentage of the relative increase in self-discharge due to the presence of H_3BO_3, RSD%, on alloy type.

4. Conclusion

- The presence of impurities in the alloy decreased the corrosion current by 33%–60% and the presence of H_3BO_3 in solution decreased the corrosion current by 59%–76%.
- Cyclic voltammetry indicated that H_3BO_3 or As, Cu, and Sb impurities in the alloy significantly suppressed the amount of large crystal $PbSO_4$ formed by the reduction peak of PbO_2.
- H_3BO_3 significantly increased the rates of oxygen and hydrogen evolution reactions for all alloys. The minimum harmful effect of H_3BO_3 is for alloy G-Cu, while the maximum harmful of H_3BO_3 is for alloy G-0.
- H_3BO_3 decreased the positive grid corrosion of all alloys (11%–44%). The impurities increased the positive grid corrosion in the absence (5%–9%) and presence of H_3BO_3 (17%–44%).
- H_3BO_3 decreased self-discharge during the reduction of all alloys (21%–41%), except for G-ACS (21% increase) and G-Cu (5% increase). The impurities increased self-discharge in the absence (31%–44%) and presence of H_3BO_3 (41%–66%).
- Under open-circuit conditions, H_3BO_3 increased significantly the self-discharge rate. The impurities increased the self-discharge rate in the absence of H_3BO_3 (44%–68%) but they decreased the rate in the presence of H_3BO_3 (11%–122%).

References

1. Maja, M.; Penazzi, N. *J. Power Sources* **1988**, *22*, 1–9.
2. Sanchez, H.; Meas; Y.; Gonzalez, I; Quiroz, M. A. *J. Power Sources* **1990**, *32*, 43–53.
3. Pavlov, D. *J. Power Sources* **1991**, *33*, 221–229.

4. Pavlov, D.; Dakhouche, A.; Rogachev, T. *J. Power Sources* **1993**, *42*, 71–88.
5. Mahato, B. K.; Tiedemann, W. H. *J. Electrochem. Soc.* **1983**, *130*, 2139–2144.
6. Hasik, E.; Paszkiewicz, M. *J. Power Sources* **1990**, *30*, 107–116.
7. Voss, E.; Hullmeine, U.; Winsel, A. *J. Power Sources* **1990**, *30*, 33–40.
8. Rogachev, T.; Pavlov, D. *J. Power Sources* **1997**, *64*, 51–56.
9. Chahmanaa, N.; Matrakovab, M.; Zerroual, L.; Pavlov, D. *J. Power Sources* **2009**, *191*, 51–57.
10. Chahmana, N.; Zerroual, L.; Matrakova, M. *J. Power Sources* **2009**, *191*, 144–147.
11. Wagner, R; Sauer, D. U. *J. Power Sources* **2001**, *95*, 141–152.
12. Bullock, K. R.; McClelland, D. H. *J. Electrochem. Soc.* **1976**, *123*, 327–331.
13. Francia, C; Maja, M; Solarino, L.; Spinelli, P.; Torcheux, L. ; Lailler, P. *J. Electrochem. Soc.* **2003**, *150*, A826–A834.
14. Amlie, R. F.; Weissman, E. Y.; Morehouse, C. K.; Qureshi, N. M. *J. Electrochem. Soc.* **1972**, *119*, 568–571 .
15. Mahato, B. K.; Weissman, E. Y.; Laird, E. C. *J. Electrochem. Soc.* **1974**, *121*, 13–16.
16. Visscher, W. J. Power Sources **1976/77**, *1*, 257–266.
17. Bullock, K. R.; McClelland, D. H. *J. Electrochem. Soc.* **1977**, *124*, 1478–1482.
18. Mahato, B. K. *J. Electrochem. Soc.* **1979**, *126*, 365–374.
19. Bullock, K. R. *J. Electrochem. Soc.* **1979**, *126*, 1848–1853.
20. Bullock, K. R. *J. Electrochem. Soc.* **1979**, *126*, 360–365.
21. Stemberg, S.; Mateescu, A.; Brânzoi, V.; Apăteanu, L. *Electrochim. Acta* **1987**, *32*, 349–351.
22. Voss, E. *J. Power Sources* **1988**, *24*, 171–184.
23. Sternberg, S.; Brânzoi, V.; Apăteanu, L. *J. Power Sources* **1990**, *30*, 177–183.
24. Garche, J.; Döring, H.; Wiesener, K. *J. Power Sources* **1991**, *33*, 213–220.
25. Döring, H.; Wiesener, K.; Garche, J.; Fischer, P. I. *J. Power Sources* **1992**, *38*, 261–272.
26. Venugopalan, S. *J. Power Sources* **1993**, *46*, 1–15.
27. Venugopalan, S. *J. Power Sources* **1994**, *48*, 371–384.
28. Meissner, E. *J. Power Sources* **1997**, *67*, 135–150.
29. Bhattacharya, A.; Basumallick, I. N. *J. Power Sources* **2003**, *113*, 382–387.
30. Paleskaa, I.; Pruszkowska-Drachala, R.; Kotowskia, J.; Dziudzia, A.; Milewskic, J. D.; Kopczykc, M.; Czerwinskia, A. *J. Power Sources* **2003**, *113*, 308–317.
31. Li, S.; Chen, H. Y.; Tang, M. C.; Wei, W. W.; Xia, Z. W.; Wu, Y. M.; Li, W. S.; Jiang, X. *J. Power Sources* **2006**, *158*, 914–919.
32. Saminathan, K.; Jayaprakash, N.; Rajeswari, B.; Vasudevan, T. *J. Power Sources* **2006**, *160*, 1410–1413.
33. Abd El-Rahman, H. A.; Salih, S. A.; Abd El-Wahab, A. M. *AFINIDAD* **2011**, *555*, 1–6
34. Abd El-Rahman, H. A.; Salih, S. A.; Abd El-Wahab, A. M. *Mat.-wiss. Werkstofftech.* **2011**, *42*, 784–791.
35. Abd El-Rahman, H. A.; Salih, S. A.; Abd El-Wahab, A. M. *Journal of Electrochemical Science and Technology* **2011**, *2*, 76–84.
36. Wei, G. L.; Wang, J. R. *J. Power Sources*, **1994**, *52*, 25–29.
37. Yazd, M. S.; Molazemi, A., Moayed, M. H. *J. Power Sources* **2006**, *158*, 705–709.
38. Badawy, W. A.; El-Egamy, S. S. *J. Power Sources* **1995**, *55*, 11–17.
39. Chen, H. Y.; Li, W. S.; Zhu, Y. B.; Tian, L. P. *J. Power Sources* **2000**, *88*, 78–82.
40. Stevenson, M. In *Encyclopedia of Electrochemical Power Sources*, Garche, J., Ed. Elsevier, Amsterdam, the Netherlands, 2009, pp. 165–178.

41. Frölich, S.; Sewig, D. *J. Power Sources* **1995**, *57*, 27–30.
42. Ellis, T. W.; Mirza, A. H. *J. Power Sources* **2010**, *195*, 4525–4529.
43. Gad-Allah, A. G.; Abd El-Rahman, H. A.; Salih, S. A.; Abd El-Galil, M. *J Appl. Electrochem.* **1995**, *25*, 682–689.
44. Gad-Allah, A. G.; Abd El-Rahman, H. A.; Salih, S. A.; Abd El-Galil, M. *J Appl. Electrochem.* **1997**, *22*, 571–756.
45. Varela, F. E.; Cordoro, E. N.; Vilche, J. R. *Electrochim. Acta* **1995**, *40*, 1183–1189.
46. Yamamoto, Y.; Matsuka, M.; Kimoto, M.; Uemura, M.; Iwakura, C. *Electrochim. Acta* **1996**, *41*, 439–444.
47. Codaro, E. N.; Vilche, J. R. *Electrochim. Acta* **1997**, *42*, 549–555.
48. Guo, Y.; Wu, M.; Hua, S. *J. Power Sources* **1997**, *64*, 65–69.
49. Guo, Y.; Wu, M.; Hua, S. *Electrochim. Acta* **1997**, *42*, 979–984.
50. Czerwiński, A.; Żelazowska, M.; Grdeń, M.; Kuc, K.; Milewski, J. D.; Nowacki, A.; Wójcik, G.; Kopczyk, M. *J. Power Sources* **2000**, *85*, 49–55.
51. Sun, Q.; Guo, Y. *J. Electroanal. Chem.* **2000**, *493*, 123–129.
52. Rocca, E.; Steinmetz, J. *J. Electroanal. Chem.* **2003**, *543*, 153–160.
53. Metikos-Hukovic, M.; Babic, R.; Brinic, S. *J. Power Sources* **2006**, *157*, 563–570.
54. McGregor, K. *J. Power Sources* **1996**, *59*, 31–43.